Fast, spatially resolved thermometry of Si and GaP crystals using pump-probe two-photon absorption

Chang-Ki Min,[a] Ji Yong Park, David G. Cahill, and Steve Granick
Department of Materials Science and Engineering and Frederick Seitz Materials Research Laboratory, University of Illinois, Urbana, Illinois 61801, USA

(Received 1 April 2009; accepted 28 May 2009; published online 8 July 2009)

Noncontact thermometry with micron-scale lateral spatial resolution and fast time resolution is shown to be enabled by measuring the temperature dependence of two-photon absorption (TPA) on crystalline semiconductors. In the proof-of-concept experiments reported here, for studies of Si, an Er:fiber laser at $\lambda = 1.56$ μm is split into pump and probe beams; where they overlap, the large TPA signal changes strongly with temperature because the two-photon energy lies between the indirect and direct bandgaps of Si. We show that the TPA coefficient increases by a factor of 2 when the temperature increases from 30 to 300 °C. For studies of GaP, we use instead a Ti:sapphire laser at 790 nm to achieve two-photon excitation above the direct bandgap. In GaP, contributions to the TPA from the dominant direct transition show less temperature dependence than for Si but the additional contribution of the indirect transition gives a similar magnitude as the temperature dependence of TPA on Si. In the current implementation using Si, the spatial resolution of the thermometry is $6 \times 6 \times 50$ μm^3 and the sensitivity is 0.6 K in a 1 kHz bandwidth. © *2009 American Institute of Physics*. [DOI: 10.1063/1.3158063]

I. INTRODUCTION

Thorough characterization of heat generation and heat transfer in microelectronic devices demands thermometry with high resolution in space and time.[1,2] Many phenomena can serve as a thermometer; all that is required is a temperature-dependent equilibrium property that can be conveniently measured. The thermometry of microelectronic and microfluidic devices is typically based on optical pyrometry. But since the wavelength of black-body infrared emission near room temperature peaks at a wavelength of 10 μm, spatial resolution is at best a few microns;[3] and moreover, since materials such as cooling water and glass absorb infrared radiation efficiently, implementation is sometimes problematic. Raman spectroscopy of the frequency, linewidth, or population of optical phonons provides higher spatial resolution but the weak cross section of Raman scattering limits the rate at which data can be acquired.[4] Thermographic phosphors are intrinsically limited in time resolution by the decay time of the phosphor.[5] Linear optical properties of semiconductors have often been used for noninvasive thermometry.[6–8] Linear optical spectroscopy also has limitations because at photon energies below or near the bandgap, the optical constants of a semiconductor depend on carrier densities; and at photon energies above the bandgap, strong optical absorption prohibits measurements within the bulk.

In this paper, we describe an alternative physical principle for thermometry within the bulk volume of a semiconductor based on the temperature dependence of two-photon absorption (TPA). For a semiconductor with an indirect bandgap, one-photon optical absorption is highly temperature dependent if the photon energy lies between the energies of the indirect and direct bandgaps because the cross section for indirect transitions involves populations of phonons that are temperature dependent.[9] The temperature dependence of TPA has not been described previously. However, it is reasonably expected to be similar to the temperature dependence of one-photon absorption when the initial and final states in the transition are the same. For the laser wavelength studied here, we confirm that Si TPA at photon energy $h\nu$ has the same temperature dependence as one-photon optical absorption at photon energy $2h\nu$.

Our work is enabled by the recent commercialization of cost-effective, high-performance fiber-laser oscillators, which generate 100 mW, 100 fs pulses at $\lambda = 1.56$ μm at the repetition rate of 100 MHz. Instead of a single-beam geometry, to further improve the sensitivity and spatial resolution, we utilize two-beam coupling in a pump-probe geometry to create a strong signal from a small volume of material in the overlap region of two beams. In the present implementation, the lateral and depth spatial resolutions are 6 and 50 μm, respectively, and data are acquired with a 2 kHz bandwidth.

II. EXPERIMENTAL DETAILS

Different light sources were used to study Si and GaP because their bandgaps differ. For Si, our pump-probe system is based on the optical design that we have used extensively for time-domain thermoreflectance and transient absorption measurements of thermal transport properties.[10,11] The main difference here is the replacement of the Ti:sapphire laser oscillator that we typically used in the past, with a 100 mW Er-fiber laser oscillator operating at a peak wavelength of 1.56 μm, a bandwidth of ≈75 nm, and a repetition rate of 100 MHz. The pump beam is modulated at 10 MHz by a $LiTaO_3$ electro-optic modulator; the modulator has a large group delay dispersion that broadens the duration of the pump optical pulse from 150 to 500 fs. Figure 1 shows the

[a]Electronic mail: ckmin@uiuc.edu.

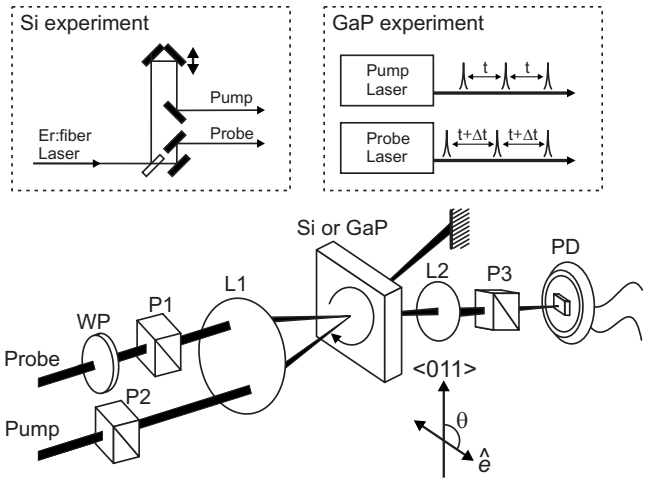

FIG. 1. Schematic drawing of the geometry used to measure the temperature, polarization, and crystal orientation dependence of TPA Si and GaP crystals. Pump and probe beams are focused within the sample using a 10× or 15× microscope objective lens (L1); after passing through the sample, the probe beam is refocused on a PD using a $f=25$ mm lens (L2). The polarization of the probe relative to the pump is controlled by a $\lambda/2$ WP and polarizers (P1 and P2). Pump scattering is removed by another polarizer (P3) when pump and probe polarizations are perpendicular. The orientation angle θ of the sample is specified by the angle between the polarization of the pump beam ($\hat{e}$) and the $\langle 011 \rangle$ direction of the crystal. The two inset figures describe the different ways that the relative delays between the pump and the probe beams are generated in the two experiments. In the Si experiment, the relative delay is adjusted by an optical delay line. In the GaP experiment, two lasers with slightly different repetition rates generate the relative delay.

measurement geometry near the sample. A 15× ($f=13.3$ mm) reflective microscope objective focuses the pump and probe to a $1/e^2$ radius of ≈ 8 μm. Because the signal arises from the product of the pump and probe intensity distributions, the lateral spatial resolution in the present implementation is $\Delta x \approx 6$ μm. The pump and probe beams intersect within the volume of a double-side polished Si wafer at an angle of 7°; the beams lie in the same plane as the probe polarization. The spatial resolution along the beam direction Δz is approximately 50 μm, which in this experiment is determined primarily by the finite spatial overlap between the noncollinear pump and probe beams, i.e., $\Delta z = \Delta x / \sin(7°)$. After passing through the wafer, the probe beam is collimated by a 25 mm focal length lens and focused onto an InGaAs photodiode (PD) detector that is placed 300 mm from the lens. The changes in the probe intensity that are correlated with the 10 MHz modulation of the pump beam are measured by a rf lock-in amplifier.

To study GaP, two Ti:sapphire lasers whose repetition rates differ by only a few tens of hertz are used as the respective light sources for the pump and probe beams.[12] For example, when the difference of repetition rate is 22 Hz, a 3.3 fs delay is generated sequentially between pump and probe pulse pairs at 82 MHz, the repetition rate of the lasers; the delay between the pump and probe is swept over a range of 12.2 ns every 45.5 ms. Both lasers generate 30 fs pulses at the center wavelength of 790 nm after compensation of group velocity dispersion using a pair of fused silica prisms.

The two laser beams are focused on the sample to a $1/e^2$ radius of ≈ 3.5 μm using a 10× ($f=20$ mm) microscope objective; see Fig. 1. The lateral spatial resolution is $\Delta x \approx 2.5$ μm. The laser power on the sample is 3 mW for the pump beam and 0.4 mW for the probe beam. In Fig. 1, the waveplate (WP) and the polarizer in the path of the probe beam are rotated together to change the polarization of the probe beam. When only the WP is rotated, the power in the probe beam can be controlled. This method has the advantage of providing better control of polarization than positioning the WP after the polarizer. After passing through the sample, the probe beam is focused onto an amplified Si detector with 100 MHz bandwidth using the same lens as for experiments on Si. The PD signal is measured using a PCI data acquisition board with an external clock and an external trigger. The external clock is generated by a second PD that measures the timing of the probe pulses and the external trigger is generated by second harmonic generation created by the coincidence of pump and probe pulses in a β-barium borate (BBO) crystal. Typically, 5000 measurements are averaged to acquire each data reported below.

TPA signals are proportional to the square of laser power. In our experiments, the correlation of pump and probe powers is measured; therefore, the TPA signal is proportional to the product of pump and probe powers. Over the power ranges that we employed, we confirmed this dependence and the absence of potential nonlinear effects such as pump depletion. Figure 2 shows the power dependences of the TPA signal as a function of the average pump power, P for Si and GaP crystals using 1.56 μm and 800 nm light sources, respectively. In Fig. 2, we plot the transient change in probe power, $\Delta\psi$ normalized by the average probe power, ψ. In the low power regime, both sets of data are well fitted with linear equations with zero intercepts, as expected for a signal created by TPA. In the experiments described below, pump powers of 88 and 3 mW are used to measure the TPA signal in Si and GaP, respectively; these pump powers are well within the regime where TPA signal is proportional to pump power.

To remove systematic errors created by drifts of the laser power, we normalize $\Delta\psi$ by the product of ψ and P; i.e., we use $\phi = \Delta\psi/(\psi P)$ to summarize our results. Therefore, ϕ, the signal normalized by the pump and the probe power, is independent of the pump and probe powers. The temperature calibration is needed only for one pump and probe power in linear region. ϕ is an experimental parameter and can be converted into a more fundamental physical parameter, the TPA coefficient, using the exact pulse shape, but that is not needed in our thermometry. The background scattering from the pump beam can be measured by adjusting the relative time delay such that the pump and probe are not temporally aligned. When calculating the TPA signal, this background is subtracted from the measurement. In the temperature calibration and measurements, we use perpendicular polarization of the pump and probe and use a polarizer to block scattered light from the pump. In this configuration, scattered light from the pump that reaches the detector is negligible. Specular reflection is ignored.

Four types of Si wafers and one GaP wafer were used in these experiments: Si (100) oriented, n-type, 1 Ω cm, thickness 1 mm; Si (100) oriented, p-type, 1 Ω cm, thickness 0.3

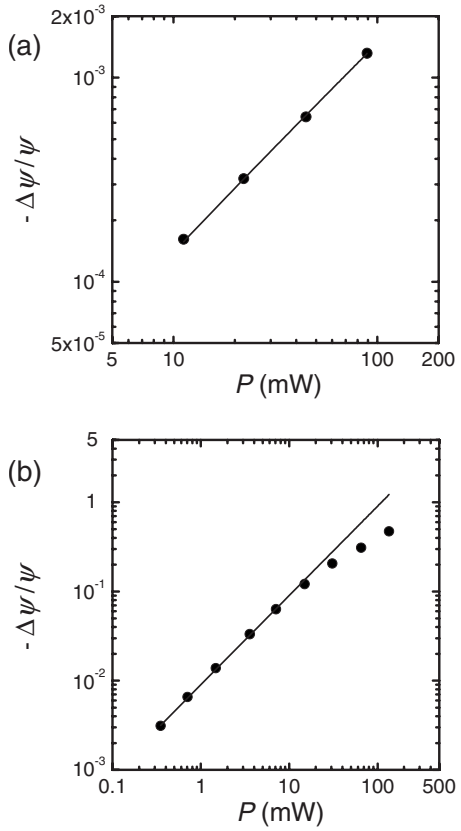

FIG. 2. Transient changes in probe power normalized by the average probe power, $\Delta\psi/\psi$, at zero delay time as a function of pump power, P, for Si [panel (a)] and GaP [panel (b)] crystals using 1.56 μm and 790 nm light sources, respectively. Pump and probe polarizations are orthogonal and pump polarizations are parallel to the $\langle 011\rangle$ direction of the crystals. The symbols are measurements and the lines are fits to linear equations with intercept=0. In Si, all data points are used to fit it, but in GaP, only five data points at low power are used.

mm; Si (111) oriented, p-type, 0.1 Ω cm, thickness 0.5 mm; Si (100) oriented, p-type, 10 Ω cm, thickness 0.5 mm; and GaP (100) oriented, n-type, 0.73 Ω cm, thickness 1 mm. The two-photon signals of all these Si samples show the same signal strength to within 2%; see Fig. 3. The data reported below refer to the first of the Si wafers listed above.

In these initial experiments, we have focused on the measurements of the changes in the intensity of the probe beam after the probe passes through a wafer. Alternatively, essentially the same temperature-dependent data can be acquired from reflections of the probe beam from the back side of a wafer. The counterpropagating pump and probe beams in a reflection geometry make the analysis of the transient absorption signal more complex but we anticipate that a reflection geometry will be easier to implement in practical applications of these ideas.

III. RESULTS AND DISCUSSION

As expected for TPA, the duration of the transient absorption signal mimics the time correlation of the pump and probe beams. This is illustrated in Fig. 4, where this quantity is plotted against the delay time between the pump and probe

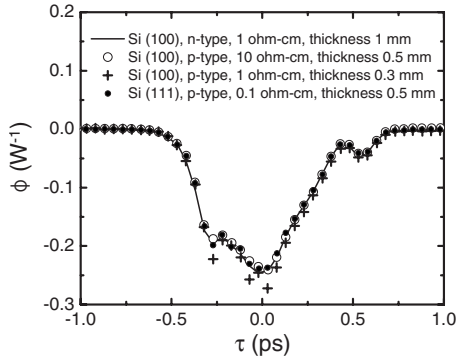

FIG. 3. Transient absorption of the probe beam as a function of the time delay between pump and probe for four types of Si crystals using the 1.56 μm light source. The data are labeled by the orientation, carrier type, resistivity, and thickness of each wafer. Laser polarizations and sample orientations are the same as Fig. 2. The signal measured by the rf lock-in is normalized by the average voltage output of a PD detector and the incident power in the pump beam; in other words, we plot $\phi=\Delta\psi/(\psi P)$, where ψ is the power in of the probe beam and P is the power of the pump beam. Near zero delay time, the fluctuations in the data for the thinnest Si wafer (0.3 mm thickness) are due to optical interference between reflections from the front and back surfaces of the wafer.

pulses. For experiments with Si, since the pump beam passes through an electro-optic modulator and the probe does not, the pump pulse has a different temporal profile than the probe and the time correlation is not symmetric in delay time. In Fig. 4, TPA time correlations of Si are slightly different from those of Fig. 3, because pulse shapes can be

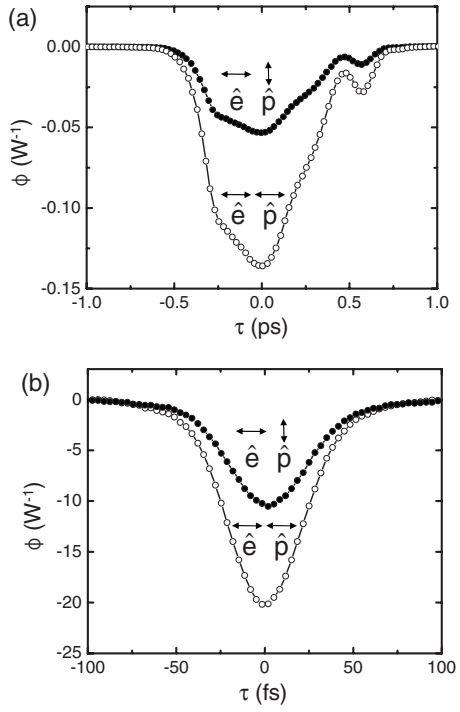

FIG. 4. Transient absorption of the probe beam as a function of the time delay between pump and probe for Si [panel (a)] and GaP [panel (b)] crystals; 1.56 μm and 790 nm light sources generate transient TPA in Si and GaP, respectively. The pump and probe powers are 88 and 2 mW in Si; and 3 mW and 0.4 mW in GaP, respectively. The pump and probe polarizations are denoted $\hat{e}$ and $\hat{p}$, respectively. In both configurations of the relative polarizations, we select the crystal orientation that produces the maximum signal.

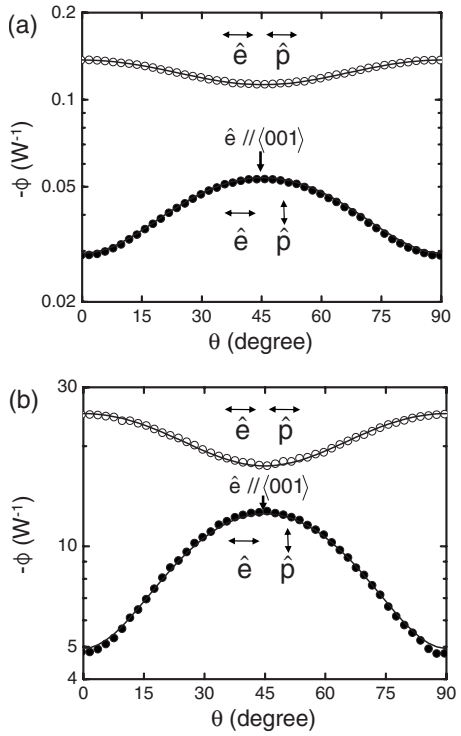

FIG. 5. Normalized transient absorption at zero delay time as a function of the orientation of the pump and probe polarizations and the orientation of the Si(001) [panel (a)] and GaP(001) [panel (b)]. The symbols are measurements and the solid lines are fits to Eqs. (1) and (2) used to determine the ratio $\mathrm{Im}\{\chi^{(3)}_{xxxx}\}/\mathrm{Im}\{\chi^{(3)}_{xyxy}\}=2.1$ in Si and $\mathrm{Im}\{\chi^{(3)}_{xxxx}\}/\mathrm{Im}\{\chi^{(3)}_{xyxy}\}=5.1$ in GaP. Maximum TPA is produced when the polarizations of the pump and probe beams are parallel and aligned along a ⟨011⟩ direction of the Si crystal. Minimum is when these polarizations, aligned along a ⟨011⟩ direction of the Si crystal, are orthogonal to one another.

different when an Er:fiber laser is operated in different regimes of mode locking. For experiments with GaP, pump and probe pulses are controlled to be almost identical so that the TPA correlation is symmetric.

In principle, other processes could contribute to the transient absorption, among them electron-hole pairs generated by TPA and one-photon optical absorption, and heating of free carriers. These potential effects appear to be negligible, as these processes would have a finite lifetime and the transient absorption at delay times longer than pulse duration are much smaller than the transient absorption near zero delay time. The temporal resolution of the data in Fig. 4 could be increased if needed by elaborating the optical setup to produce shorter pulses.

Previously, *isothermal* TPA in GaAs and CdTe was studied by Dvorak *et al.*[13] using two-beam coupling. TPA is controlled by the imaginary part of the third-order susceptibility tensor $\chi^{(3)}$. For cubic crystals of space group 432, $m3m$, or $\bar{4}3m$, the $\chi^{(3)}$ tensor has three unique components: $\chi^{(3)}_{xxxx}$, $\chi^{(3)}_{xyxy}$, and $\chi^{(3)}_{xxyy}$ in a degenerate case; Dvorak *et al.*[13] showed how these three components can be determined from the data for the changes in TPA as a function of the polarizations of the pump and probe beams and their orientations relative to the crystallographic axes. Figure 5 shows our data for TPA in Si and GaP for beams propagating along directions close to the ⟨001⟩ crystallographic axis. For this geometry, Eqs. (23) and (24) of Ref. 13 simplify to

$$\phi(\theta) = -3\sqrt{\frac{\sigma_1^2}{\sigma_1^2+\sigma_2^2}}\frac{\omega l_{\mathrm{eff}}\Gamma}{\varepsilon_0 n^2 c^2 \pi \omega_0^2} \times \mathrm{Im}\left\{\chi^{(3)}_{xxxx} - \frac{\chi^{(3)}_{xxxx}-\chi^{(3)}_{xxyy}-2\chi^{(3)}_{xyxy}}{2}\cos^2 2\theta\right\}, \tag{1}$$

$$\phi(\theta) = -3\sqrt{\frac{\sigma_1^2}{\sigma_1^2+\sigma_2^2}}\frac{\omega l_{\mathrm{eff}}\Gamma}{\varepsilon_0 n^2 c^2 \pi \omega_0^2} \times \mathrm{Im}\left\{\chi^{(3)}_{xyxy} + \frac{\chi^{(3)}_{xxxx}-\chi^{(3)}_{xxyy}-2\chi^{(3)}_{xyxy}}{2}\cos^2 2\theta\right\}. \tag{2}$$

Equation (1) applies when the pump and probe have parallel polarization and Eq. (2) applies when the pump and probe are cross polarized. Here σ_1 and σ_2 are pulse widths of pump and probe pulses, ω is the angular frequency, l_{eff} is the effective length of interaction, Γ is the ratio of pump peak power to average power, ω_0 is the $1/e^2$ radius of the beam, n is the refractive index, c is speed of light, ε_0 is the permittivity of free space, and θ is the angle between the polarization of the pump beam and the ⟨011⟩ direction of the Si crystal. The fits of these equations are shown in Fig. 5. In Si, the independent $\chi^{(3)}$ tensors are reduced to $\chi^{(3)}_{xxxx}$ and $\chi^{(3)}_{xyxy}$ ($\chi^{(3)}_{xyxy} \approx \chi^{(3)}_{xxyy}$) because the optical transitions are far from Si resonances.[14] The fit of these equations to the data in Fig. 3(a) gives $\mathrm{Im}\{\chi^{(3)}_{xxxx}\}/\mathrm{Im}\{\chi^{(3)}_{xyxy}\}=2.1$ for Si. This same degree of anisotropy is observed in third-harmonic generation using $\lambda=1.56$ μm laser light.[15] Zhang *et al.*[16] found a comparable degree of anisotropy for both TPA and the Kerr nonlinearity using single-beam measurements. In Fig. 5(b), the fit of equations to the data gives $\mathrm{Im}\{\chi^{(3)}_{xxxx}\}/\mathrm{Im}\{\chi^{(3)}_{xyxy}\}=5.1$ and $|\mathrm{Im}\{\chi^{(3)}_{xxyy}\}/\mathrm{Im}\{\chi^{(3)}_{xyxy}\}|<0.06$ for GaP. Here the error bars are estimated from the angle between the laser and surface, which cannot be avoided because of the finite angle between the pump and probe pulses.

The main point is that TPA in Si is strongly temperature dependent when two-photon energy is between the indirect and direct bandgaps of Si, as Fig. 6(a) demonstrates. Since the initial and the final states of transitions are the same and the density of state of the intermediate state of the TPA transition is near zero, we can reasonably expect that TPA will have the same temperature dependence as one-photon absorption at the two-photon energy used in our experiments, $\lambda=780$ nm or equivalently 1.59 eV. For Si, 1.6 eV lies above the indirect bandgap of $E_g=1.1$ eV and below the direct bandgap of 3.4 eV; therefore, photoexcitation of an electron-hole pair by a 1.6 eV photon (or by two 0.8 eV photons) requires the absorption or emission of a phonon. Higher temperatures produce greater phonon populations and stronger optical absorption. Phonons from more than one branch contribute to the process.[17,18] The one-photon optical absorption $A(h\nu, T)$ as a function of photon energy $h\nu$ and temperature T is given by[17,18]

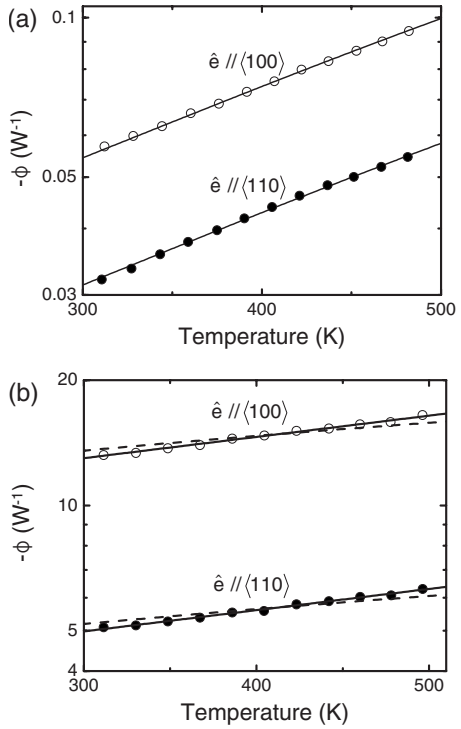

FIG. 6. Temperature dependence of the TPA for perpendicular polarizations of the pump and probe aligned along the ⟨001⟩ and ⟨011⟩ directions of Si [panel (a)] and GaP [panel (b)] crystals. The laser source is an Er:fiber laser operating at a center wavelength of 1.56 μm [panel (a)] and a Ti:sapphire laser operating at a center wavelength of 790 nm [panel (b)]. The symbols denote measurements. For Si, solid lines, which appear linear on these axes to the eye, are fits to Eq. (3) using one fitting parameter, the constant of proportionality, D. For GaP, the dashed lines are fits to Eq. (4); the differences between the dashed lines and the data are attributed to contributions to the absorption from indirect transitions. The solid lines in panel (b) are fits to Eq. (5).

$$A(h\nu,T) = D\sum_{i=1}^{4} P_i \left[\frac{[h\nu - E_g(T) + \varepsilon_i]^2}{\exp(\varepsilon_i/kT) - 1} + \frac{[h\nu - E_g(T) - \varepsilon_i]^2}{1 - \exp(-\varepsilon_i/kT)} \right]. \quad (3)$$

Four phonons with energies of $\varepsilon_i/k = 212$, 670, 1050, and 1420 K are included in this calculation; the coupling constants are $P_1 = 0.033$, $P_2 = 1$, $P_3 = 0.063$, and $P_4 = 0.063$. Here D is a fitting parameter and $E_g(T)$ is obtained from Ref. 18. Figure 6(a) shows the comparison between the predictions of Eq. (3) and the data. We use the data acquired with perpendicular pump-probe polarizations to reduce the influence of diffuse scattering from pump beam. The agreement between this model and the data is excellent for both orientations of the Si crystal.

TPA has a weak temperature dependence when the two-photon energy is greater than the direct bandgap as shown for GaP (100) in Fig. 6(b). In this case, the one-photon energies (centered at 1.57 eV) are below the indirect bandgap of 2.26 eV and the two-photon energies are above the direct bandgap of 2.76 eV. One-photon absorption for an allowed transition at energies above the direct bandgap is typically well described by[9]

$$A(h\nu,T) = D'\sqrt{h\nu - E_g(T)}. \quad (4)$$

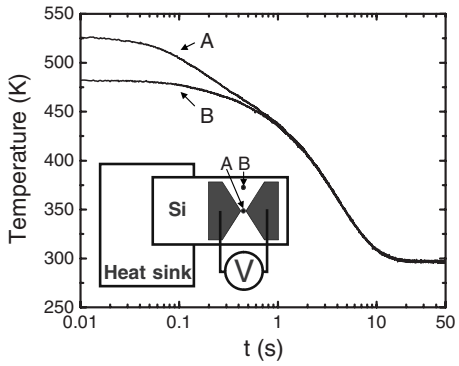

FIG. 7. Temperature, measured at two spots relative to a resistive heater as indicated in the schematic in the figure inset, is measured as a function of time after heating, 10 ms–50 s, at two points separated by 5 mm along a Si strip. A Cr layer with 120 nm thickness is used as the electrical contact; the gap between the contacts is 2 mm.

In Fig. 6(b), we compare the data to the predictions of Eq. (4) using previously published data for $E_g(T)$.[19] The difference between the fit and the data can be explained by a contribution to the absorption from indirect transitions. We estimate the strength of the indirect transition at 300 K as 10% of the strength of the direct transition,[20] and estimate that the strength of the indirect transition increases by approximately 100% when the temperature is increased from 300 to 500 K, similar to what [Fig. 6(a)] we observe in Si.

A robust calibration for thermometry based on TPA follows from these considerations. For temperatures between 300 and 500 K, the dependence of ϕ on temperature T can be empirically approximated by $\phi = \phi_0 \exp(T/T_0)$. Solving for temperature T gives

$$T = T_0 \ln\left(\frac{\phi}{\phi_0}\right), \quad (5)$$

which fits the experimental data nicely using the parameters $T_0 = 328$ K and $\phi_0 = 0.0127$ and 0.0218 W^{-1} for the two orientations of the crystal. The fit of the data to Eq. (5) is indistinguishable from the fit of the data to Eq. (3); see Fig. 6.

Next, we demonstrate an implementation of this thermometry to measure temperature distributions. TPA thermometry was performed on a strip of Si wafer heated by a pulse of electrical current passing between two thin-film Cr electrodes. The decay of temperature after heating, not just at the center of the heat source (point A) but also at 5 mm removed from the center of the heat source (point B), is shown in Fig. 7. In this example, we used a 100 μs time constant at the output stage of the rf lock-in; therefore, the bandwidth of the measurement is $\approx$2 kHz. At the end of the heating pulse (80 V applied for 2 s), the temperature at point A is $\approx$50 K higher than the temperature at point B. This temperature difference decays with a time constant of $\approx$0.3 s, as expected since the thermal diffusivity of Si at these temperatures is $D \approx 0.5$ cm^2/s and $(5\ \text{mm})^2/(2D) \approx 0.25$ s. An analysis of the noise in this experiment shows that the rms variation in this measurement of temperature is $\approx$0.6 K in a 1 kHz bandwidth. Because of low frequency noise in our apparatus, noise does not scale with the square root of the

bandwidth and improves to only ≈0.2 K in a 1 Hz bandwidth. Tighter focusing of the beams would result in both higher spatial resolution and lower noise.

Heating of the Si substrate by TPA is negligible in this demonstration of Si temperature measurement. The problem of local heating in the probe area can be considered on time scales that are short and long compared to the laser repetition rate. In the short time regime, heating by each pump and probe pulse creates a transient temperature rise. The instantaneous temperature rise by a single pair of pump and probe pulses is estimated to be 0.5 mK by

$$\frac{E_a}{\pi \omega_0{}^2 z_R C}, \tag{6}$$

where $E_a = 80$ pJ is the absorbed energy by a single pump pulse, $\omega_0 = 8$ μm is the $1/e^2$ beam radius, $z_R = 460$ μm is the Rayleigh length in Si, and $C = 1.62$ J/cm^3 K is the volumetric heat capacity. In the long time regime, accumulation of heat from multiple optical pulses is dissipated by conduction into the surrounding crystal. The steady-state temperature rise is calculated to be 40 mK by

$$\frac{P_a}{2\pi z_R \Lambda} \ln\left(\frac{z_R}{\omega_0}\right), \tag{7}$$

where $P_a = 4$ mW is the absorbed power and $\Lambda = 142$ W/m K is the thermal conductivity of Si. Shorter pulse durations will reduce the local heating while maintaining the same signal strength.

IV. CONCLUSIONS

The transient absorption of Si near zero delay time, which arises from TPA, displays temperature dependence in excellent agreement with theory and therefore enables noncontact thermometry with a temperature calibration based on well-understood solid-state physics of Si. This physics is general and, if the laser wavelength can be chosen appropriately, should be applicable to any semiconductor with an indirect bandgap, e.g., GaP, Ge, and SiC, but would not be expected to apply to amorphous materials or semiconductors where the optical absorption is dominated by a direct transition.

ACKNOWLEDGMENTS

The authors thank Dr. Sung Chul Bae for many discussions and gratefully acknowledge financial support from the taxpayers of the United States through the Office of Naval Research MURI program, Grant No. N00014-07-1-0723.

[1] D. G. Cahill, W. K. Ford, K. E. Goodson, G. D. Mahan, A. Majumdar, H. J. Maris, R. Merlin, and S. R. Phillpot, J. Appl. Phys. **93**, 793 (2003).
[2] P. K. Schelling, L. Shi, and K. E. Goodson, Mater. Today **8**, 30 (2005).
[3] D. P. DeWitt and G. D. Nutter, *Theory and Practice of Radiation Thermometry* (Wiley Interscience, New York, 1988).
[4] T. Beechem, S. Graham, S. Kearney, L. Phinney, and J. Serrano, Rev. Sci. Instrum. **78**, 061301 (2007).
[5] S. W. Allison and G. T. Gillies, Rev. Sci. Instrum. **68**, 2615 (1997).
[6] K. Postava, M. Aoyamaa, J. Mistrika, T. Yamaguchia, and K. Shiod, Appl. Surf. Sci. **254**, 416 (2007).
[7] J. Heller, J. W. Bartha, C. C. Poon, and A. C. Tam, Appl. Phys. Lett. **75**, 43 (1999).
[8] J. C. Sturm and C. M. Reaves, IEEE Trans. Electron Devices **39**, 81 (1992).
[9] R. A. Smith, *Semiconductors* (Cambridge University Press, Cambridge, 1978).
[10] D. G. Cahill, Rev. Sci. Instrum. **75**, 5119 (2004).
[11] D. G. Cahill, K. E. Goodson, and A. Majumdar, ASME J. Heat Transfer **124**, 223 (2002).
[12] A. Bartels, R. Cerna, C. Kistner, A. Thoma, F. Hudert, C. Janke, and T. Dekorsy, Rev. Sci. Instrum. **78**, 035107 (2007).
[13] M. D. Dvorak, W. A. Schroeder, D. R. Andersen, A. L. Smirl, and B. S. Wherrett, IEEE J. Quantum Electron. **30**, 256 (1994).
[14] J. J. Wynne, Phys. Rev. **178**, 1295 (1969).
[15] D. J. Moss, H. M. van Driel, and J. E. Sipe, Opt. Lett. **14**, 57 (1989).
[16] J. Zhang, Q. Lin, G. Piredda, R. W. Boyd, G. P. Agrawal, and P. M. Fauchet, Appl. Phys. Lett. **91**, 071113 (2007).
[17] E. H. Sin, C. K. Ong, and H. S. Tan, Phys. Status Solidi A **85**, 199 (1984).
[18] G. G. Macfarlane, T. P. McLean, J. E. Quarington, and V. Robets, Phys. Rev. **111**, 1245 (1958).
[19] T. Takizawa, J. Phys. Soc. Jpn. **52**, 1057 (1983).
[20] P. J. Dean, G. Kaminsky, and R. B. Zetterstrom, J. Appl. Phys. **38**, 3551 (1967).